# The influence of wall suction and blowing on boundary-layer laminar streaks generated by free-stream vortical disturbances

Pierre Ricco and Fahad Dilib
*Department of Mechanical Engineering, King's College London, Strand, London, WC2R 2LS United Kingdom*
(Dated: May 7, 2010)

The effect of mean-flow wall transpiration on boundary-layer fluctuations generated by free-stream disturbances of the convected gust type is investigated numerically. The theoretical frameworks of S.J. Leib, D.W. Wundrow, & M.E. Goldstein [J. Fluid Mech., 380, 169, (1999)] and P. Ricco [J. Fluid Mech., 638, 267, (2009)], based on the linearized unsteady boundary-region equations, are adopted. It is found that wall suction has a more significant attenuating effect on the low-frequency laminar streaks, while high-frequency disturbances are brought closer to the wall, but unaffected in magnitude. A simple asymptotic result, confirmed by the numerical calculations, shows that the characteristic peak of the laminar streaks in the core of the boundary layer may be suppressed completely by suction if this is sufficiently intense. Thought experiments of the modification induced by suction on existing wind-tunnel root-mean-square data are carried out. The findings are compared with other laboratory data with wall suction and the reasons for discrepancy are outlined.

## I. INTRODUCTION

**Published in Phys. Fluids, 22, 044101 (2010).**

The instability of laminar boundary layers and their transition to turbulence are important phenomena in many engineering flow systems. Researchers have studied these occurrences for decades, focussing on how external agents, such as free-stream fluctuations and wall roughness, induce boundary-layer disturbances and on whether the latter become unstable and lead to the laminar flow breakdown[1]. One of the main challenges is to extend the laminar region and to delay transition to reduce the overall friction. An efficient technique to achieve this is the application of steady wall suction to attenuate the boundary-layer disturbances. Joslin[2] presents an extensive review on laminar flow control, mainly discussing design issues for wall suction in aeronautical applications.

The present work deals with the effects of distributed steady wall suction and blowing on a Blasius boundary layer perturbed by low-frequency, streamwise-elongated vortical disturbances induced by free-stream vortical perturbations. This is a problem of vast academic and engineering interest because such fluctuations occur in numerous fluid systems, such as over aircraft wings and turbine blades. These streaks, often called Klebanoff or breathing modes, are especially energetic in the presence of medium-to-high free-stream turbulence and may break down to turbulent spots through a secondary instability mechanism[3]. This phenomenon is usually referred to as bypass transition because the unstable Tollmien-Schlichting (TS) waves predicted by the classical stability theory may not play a decisive role.

Early studies on the laminar streaks were conducted in low-speed wind tunnels by Dryden[4] and Taylor[5]. They showed that the boundary-layer streamwise perturbations were of low frequency and reached amplitudes much larger than in the free stream. After about thirty years of research focussed on TS waves, the interest on fluctuations generated by medium and high free-stream disturbances was revived by Klebanoff's experiment[3]. Further relevant laboratory investigations by Westin *et al.*[6] and Matsubara & Alfredsson[7] (amongst many) have showed that these streamwise-elongated perturbations peak in the core of the boundary layer and that the streamwise velocity component is much larger than both the wall-normal and spanwise velocity components. Direct numerical simulations have also appeared[8,9], and have largely confirmed the experimental findings.

The mathematically rigorous approach describing the dynamics of the laminar streaks has been developed by Leib, Wundrow, & Goldstein[10] (LWG), Wundrow & Goldstein[11], and Wu & Choudhari[12]. These formulations are based on the boundary-layer and boundary-region equations, i.e. the asymptotic limits of the Navier-Stokes equations for low frequency disturbances. The method of matched

asymptotic expansion has been used to obtain the initial and outer boundary conditions, which synthesize the mutual interaction between the perturbations within the viscous layer and in the free stream. The boundary layer has been found to act as a low-pass filter, namely low-frequency free-stream perturbations penetrate into the boundary layer and amplify downstream, while the high-frequency ones confine in an edge layer, located near the free stream. LWG's approach has been extended to the compressible regime by Ricco & Wu[13] and Ricco, Tran & Ye[14], where the effect of wall-heat transfer on thermal Klebanoff modes and on oblique TS-waves was studied. While LWG's analysis captures the dynamics of the streamwise velocity fluctuations in the core of the boundary layer, allowing this velocity component to vanish in the free stream, Ricco[15] (R09) recently computed the streak signature in the outer portion of the boundary layer, thereby attaining the streamwise velocity profile of the Klebanoff modes along the whole wall-normal extent. The streak profiles compared successfully with the experimental data by Westin *et al.*[6] and pressure disturbances have been found to play a key role in the outer layer dynamics (see also Ricco[16]).

The experimental works on the influence of wall suction on the laminar streaks are limited. Fransson & Alfredsson[17] and Yoshioka, Fransson, & Alfredsson[18] carried out wind-tunnel experiments on streaks evolving in the asymptotic suction boundary layer (ASBL) and showed that the perturbations were significantly suppressed. Laminar boundary layers with mean-flow suction (mostly ASBL) disturbed by laminar streaks have been studied numerically by Levin, Davidsson, & Henningson[19] via direct numerical simulations, by Davidsson & Gustavsson[20] by the linearized Navier-Stokes equations, and by Fransson & Corbett[21], Zuccher, Luchini, & Bottaro[22], and by Bystrom *et al.*[23] through optimal growth theory.

In the present work, the theoretical framework of R09 is employed to study the influence of distributed steady wall transpiration on the evolution of unsteady two- and three-dimensional vorticity disturbances engendered by free-stream convective gusts. The main difference with previous works resides in the fact that herein the laminar streaks are generated by the continuous, external forcing action of the free-stream vortical disturbances, as highlighted by experimental evidence[7]. On the contrary, other studies have adopted iterative methods[19,21–23] or localized initial conditions[20] to generate the streaks, and have neglected free-stream vortical fluctuations, which are responsible for the formation and evolution of the laminar streaks. Furthermore, studies based on optimal theory treat the streaks as steady, whereas the effect of the frequency of the free-stream perturbations is considered here. Joslin[2] at page 13 remarks that receptivity theory has never been employed for laminar flow control research, and that such an effort would be an extremely relevant contribution for transition prediction. The present work can therefore be considered a first step in this area of boundary-layer control.

The intensity of the transpiration is strong enough to modify the Blasius mean flow, while the amplitude of the streaks is assumed small so that the equations are linearized about the mean flow. We first study how wall suction and blowing affect velocity perturbations induced by a two-dimensional convected gust with a wall-normal wavelength larger than and comparable with the boundary-layer thickness. We then investigate the same effect on the three-dimensional Klebanoff modes and use asymptotic analysis to obtain an analytical expression for the velocity profiles in the limit of large suction. We employ LWG's theory and the procedure outlined in R09 at pages 22-25 to compute the evolution of the full spectrum of laminar streaks, and we compare the results with experimental data.

The paper is structured as follows. The mathematical formulation and the numerical procedures are presented in §II. Section §III discusses the influence of wall transpiration on the boundary-layer vorticity signatures induced by a two-dimensional gust (§III A), by a single three-dimensional gust (Klebanoff mode) and by full-spectrum free-stream turbulence (§III B). A summary and a list of ideas for future work are given in §IV.

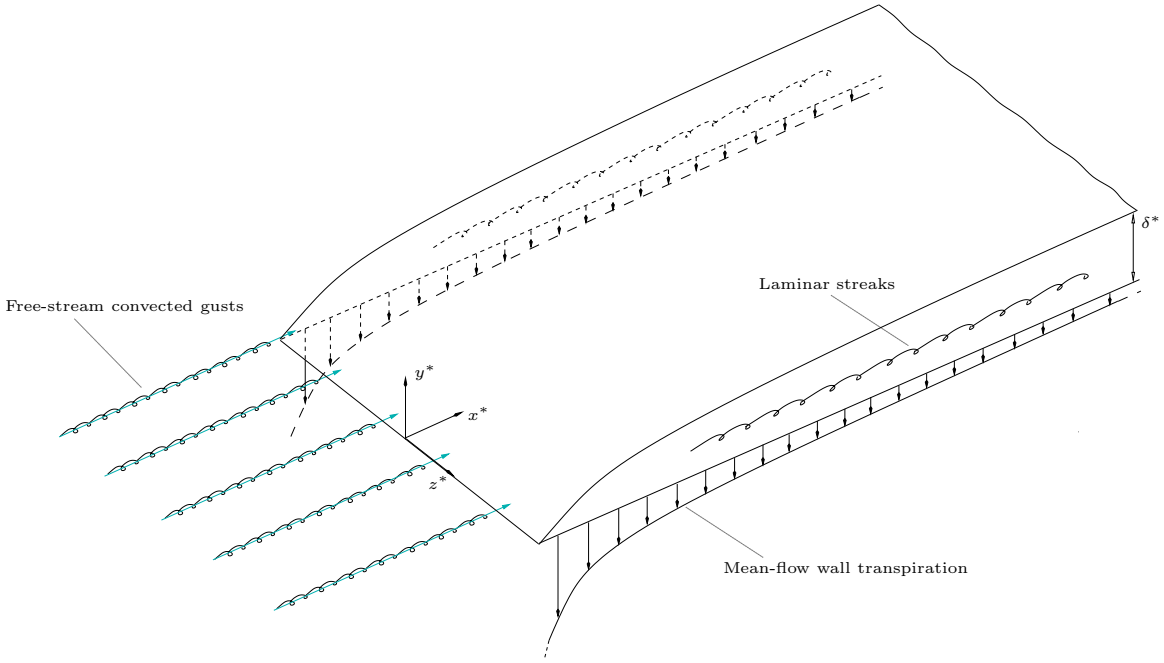


FIG. 1: Schematic of the physical domain.

## II. MATHEMATICAL FORMULATION

The mathematical framework is based on the works by R09 and LWG, adapted to include steady wall transpiration. We consider a uniform, incompressible free-stream flow with velocity $U_\infty$ past an infinitely thin plate. Homogeneous, statistically-stationary vortical disturbances are superimposed on the mean free-stream flow. The disturbances are of the convective gust type, i.e. they are advected at $U_\infty$. The flow is described in terms of a Cartesian coordinate system, i.e. by $\mathbf{x} = x\hat{\mathbf{i}} + y\hat{\mathbf{j}} + z\hat{\mathbf{k}}$, where $x, y$ and $z$ denote the streamwise, wall-normal and spanwise directions, scaled by the gust spanwise wavelength $\lambda_z^*$. The streamwise coordinate is non-dimensionalized by the gust streamwise wavenumber $k_x^* = 2\pi/\lambda_x^*$, namely $\overline{x} = 2\pi x^*/\lambda_x^* = \mathcal{O}(1)$. The wall-normal coordinate is scaled by $\delta^* = \sqrt{2x^*\nu^*/U_\infty}$ ($\nu^*$ is the kinematic viscosity of the fluid), a measure of the thickness of the boundary layer in the no-transpiration case, so that $\eta = y^*/\delta^* = \mathcal{O}(1)$ (see (3)). The velocities are non-dimensionalized by $U_\infty$ and pressure by $\rho^* U_\infty^2$, where $\rho^*$ is the free-stream density. The symbol $^*$ indicates a dimensional quantity. A schematic of the physical domain is displayed in figure 1.

The free-stream vorticity fluctuations are written as a superposition of sinusoidal disturbances:

$$\mathbf{u} - \hat{\mathbf{i}} = \epsilon \hat{\mathbf{u}}^\infty \mathrm{e}^{i(\mathbf{k}\cdot\mathbf{x} - k_x t)} + c.c.,$$

where $\epsilon \ll 1$ indicates the gust amplitude, $\hat{\mathbf{u}}^\infty = \{\hat{u}_x^\infty, \hat{u}_y^\infty, \hat{u}_z^\infty\}$, $\mathbf{k} = \{k_x, k_y, k_z\}$, where the wavenumbers are scaled by $\lambda_z^*$, and *c.c.* is the complex conjugate. We focus on low-frequency disturbances with $k_x \ll k_y, k_z$ as these penetrate the most into the boundary layer to form the laminar streaks. A Reynolds number is defined as $R_\lambda \equiv U_\infty \lambda_z^*/\nu \gg 1$. It occurs that

$$|\hat{\mathbf{u}}^\infty| = \sqrt{\left(\hat{u}_x^\infty\right)^2 + \left(\hat{u}_y^\infty\right)^2 + \left(\hat{u}_z^\infty\right)^2} = 1, \tag{1}$$

and the continuity equation can be written as

$$\hat{\mathbf{u}}^\infty \cdot \mathbf{k} = 0. \tag{2}$$

We focus on downstream locations where $\delta^* = \mathcal{O}(\lambda_z^*)$, i.e. where $x/R_\lambda = \mathcal{O}(1)$, which means that the spanwise diffusion is of the same order as that in the wall-normal direction. A distinguished scaling is $k_x = \mathcal{O}\left(R_\lambda^{-1}\right)$, because the laminar streaks evolve downstream on a length scale which is comparable with the gust streamwise wavelength. Due to the disparity between the spanwise and streamwise scales, $\mathcal{O}(\epsilon)$ free-stream fluctuations generate $\mathcal{O}(\epsilon/k_x)$ streamwise velocity disturbances in the boundary layer. We assume that the disturbance amplitude within the boundary layer is much smaller than the mean flow amplitude in order to linearize the equations. The condition for linearization is therefore $\epsilon/k_x \ll 1$ or $\epsilon R_\lambda \ll 1$.

The similarity variable for the boundary-layer flow, also known as the Blasius variable, is

$$\eta \equiv y\left(\frac{R_\lambda}{2x}\right)^{1/2} = y^*\sqrt{\frac{U_\infty}{2\nu x^*}}. \tag{3}$$

The mean flow solution is expressed as

$$U = F'(\eta), \quad V = -(2xR_\lambda)^{-1/2}\left(F - \eta F'\right),$$

where $U$ and $V$ represent the streamwise and wall-normal velocity components, and the prime indicates differentiation with respect to $\eta$. The $x$-momentum equation governing $F$ is

$$F''' + FF'' = 0. \tag{4}$$

The boundary conditions are

$$F(0) = F_w, \ F'(0) = 0, \ \text{and} \ F \to \overline{\eta} = \eta - \beta \ \text{as} \ \ \eta \to \infty. \tag{5}$$

The first boundary condition synthesizes the wall transpiration. The wall velocity is

$$V_w = -F_w\left(2xR_\lambda\right)^{-1/2}, \tag{6}$$

namely $F_w > 0$ for suction and $F_w < 0$ for blowing. Such a distribution of wall transpiration guarantees the similarity form of the mean-flow boundary layer, and $F_w$ alone defines the transpiration intensity. This flow is used to implement wall suction and blowing in the mathematical framework of R09. It would have been more involved to study the ASBL, despite its simple analytical formula downstream (see Schlichting & Gersten[24] at pages 307-308). This is because of the non-similar character of the ASBL flow during the initial stage of evolution from the leading edge, which would have complicated the mathematical treatment of the penetration of the free-stream vortical disturbances into the boundary layer. Studies based on optimal growth theory have almost exclusively employed the ABSL because the issue of the interaction between the viscous region and the free-stream disturbances is absent there, as the latter are not retained in the model.

For large wall suction ($F_w \gg 1$), the boundary layer becomes very thin ($\eta \ll 1$). A new wall-normal coordinate is defined, $N = -V_w^* y^*/\nu^* = F_w\eta = \mathcal{O}(1)$, and the mean flow equations simplify to[24]:

$$\frac{\partial V}{\partial N} = 0, \frac{\partial U}{\partial N} + \frac{\partial^2 U}{\partial N^2} = 0.$$

An analytical solution is found:

$$U = F'_{asy} = 1 - \mathrm{e}^{-F_w\eta}, V = V_w. \tag{7}$$

By integrating the above and by using the first condition in (5), one finds

$$F = \eta + \frac{F_w^2 - 1 + \mathrm{e}^{-F_w\eta}}{F_w},$$

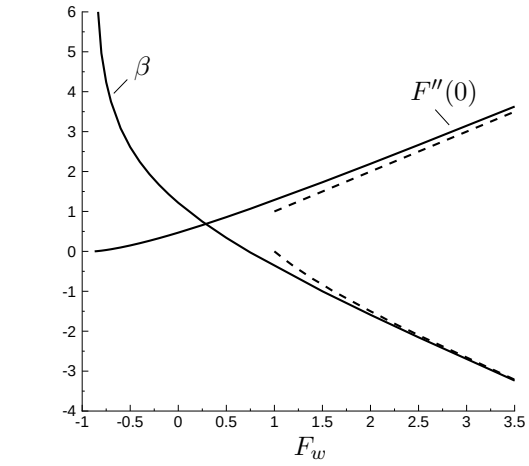


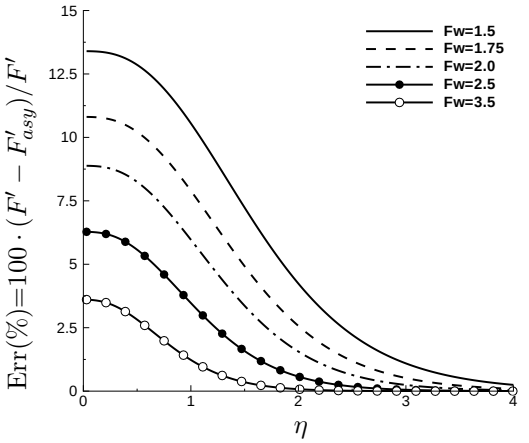


FIG. 2: Top: dependence of $\beta$ and $F''(0)$ on $F_w$. The solid lines indicate the numerical solutions, while the dashed lines denote the asymptotic solutions for $F_w \gg 1$ found from (7) for $F''(0)$ and for $\beta$ (see (8)). Bottom: Percent error between the numerical solution to (4) and the asymptotic solution (7) for different $F_w$.

and the displacement constant $\beta$:

$$\beta = \lim_{\eta\to\infty} (\eta - F)|_{F_w\gg 1} = \frac{1-F_w^2}{F_w}. \tag{8}$$

Figure 2 (top) shows the numerical and asymptotic solutions of $\beta$ and $F''(0)$ as functions of $F_w$. For massive blowing, i.e. for $F_w \to -0.8757$, $\beta \to \infty$ and $F''(0) \to 0$, for which the boundary-layer approximation becomes invalid[25]. In figure 2 (bottom), the percent difference between the numerical Blasius solution to (4) and the asymptotic solution (7) is shown to decrease as $F_w$ increases.

The boundary-layer mean flow and the disturbance solutions are expressed as:

$$\{u, v, w, p\} = \{U, V, 0, -1/2\}$$

$$+\epsilon \left\{ \overline{u}_0(\overline{x},\eta), \left(\frac{2\overline{x}k_x}{R_\lambda}\right)^{1/2} \overline{v}_0(\overline{x},\eta), \overline{w}_0(\overline{x},\eta), \overline{p}_0(\overline{x},\eta) \right\} \mathrm{e}^{i(k_z z - k_x t)} \; + \; c.c. + \ldots \tag{9}$$

The velocity and pressure disturbances are written as[15,26]

$$\left.\begin{aligned}\{\overline{u}_0,\overline{v}_0\} &= C^{(0)}\left\{\overline{u}^{(0)},\overline{v}^{(0)}\right\}+(ik_z/k_x)C\{\overline{u},\overline{v}\},\\ \overline{w}_0 &= -(ik_x/k_z)C^{(0)}\overline{w}^{(0)}+C\overline{w},\\ \overline{p}_0 &= (k_x/R_\lambda)C^{(0)}\overline{p}^{(0)}+i\kappa_z\left(k_x/R_\lambda\right)^{1/2}C\overline{p},\end{aligned}\right\} \tag{10}$$

where $\kappa_z \equiv k_z/(k_xR_\lambda)^{1/2}=\sqrt{2\pi\nu\lambda_x^*/U_\infty}/\lambda_z^*=\mathcal{O}(1)$, $C^{(0)}{=}\hat{u}_x^\infty+ik_x\hat{u}_y^\infty/\Gamma$, $C{=}\hat{u}_z^\infty+ik_z\hat{u}_y^\infty/\Gamma$, and $\Gamma=\sqrt{k_x^2+k_z^2}$.

The linearized unsteady boundary-region equations (LUBR) describe the disturbance dynamics. They represent the asymptotically rigorous limit of the Navier-Stokes equations for disturbances with $k_x^*/k_z^*\to 0$ at $\overline{x}=\mathcal{O}(1)$, i.e. with a streamwise wavelength which is long compared with both the boundary-layer thickness and the spanwise wavelength[27]. In this limit, the first-order terms in (10) are proportional to $\{\overline{u},\overline{v},\overline{w},\overline{p}\}$, while the second-order terms, i.e. $\mathcal{O}(k_x^*/k_z^*)$ smaller than the leading-order ones, are the ones proportional to $\{\overline{u}^{(0)},\overline{v}^{(0)},\overline{w}^{(0)},\overline{p}^{(0)}\}$. The LUBR equations are well suited for studying the laminar streaks because experimental evidence[6] indicates that these structures are streamwise-elongated and their spanwise wavelength is $\mathcal{O}(\delta^*)$. Both $\{\overline{u}^{(0)},\overline{v}^{(0)},\overline{w}^{(0)},\overline{p}^{(0)}\}$ and $\{\overline{u},\overline{v},\overline{w},\overline{p}\}$ satisfy the LUBR equations:

$$\frac{\partial\overline{u}}{\partial\overline{x}}-\frac{\eta}{2\overline{x}}\frac{\partial\overline{u}}{\partial\eta}+\frac{\partial\overline{v}}{\partial\eta}+\overline{w}=0, \tag{11}$$

$$\left(-i+\kappa_z^2-\frac{\eta F''}{2\overline{x}}\right)\overline{u}+F'\frac{\partial\overline{u}}{\partial\overline{x}}-\frac{F}{2\overline{x}}\frac{\partial\overline{u}}{\partial\eta}-\frac{1}{2\overline{x}}\frac{\partial^2\overline{u}}{\partial\eta^2}+F''\overline{v}=0, \tag{12}$$

$$\left(-i+\kappa_z^2+\frac{(\eta F')'}{2\overline{x}}\right)\overline{v}+F'\frac{\partial\overline{v}}{\partial\overline{x}}-\frac{F}{2\overline{x}}\frac{\partial\overline{v}}{\partial\eta}-\frac{1}{2\overline{x}}\frac{\partial^2\overline{v}}{\partial\eta^2}-\frac{\eta(\eta F')'-F}{(2\overline{x})^2}\overline{u}+\frac{1}{2\overline{x}}\frac{\partial\overline{p}}{\partial\eta}=0, \tag{13}$$

$$\left(-i+\kappa_z^2\right)\overline{w}+F'\frac{\partial\overline{w}}{\partial\overline{x}}-\frac{F}{2\overline{x}}\frac{\partial\overline{w}}{\partial\eta}-\frac{1}{2\overline{x}}\frac{\partial^2\overline{w}}{\partial\eta^2}-\kappa_z^2\overline{p}=0. \tag{14}$$

The outer (free-stream) boundary conditions are (R09)

$$\overline{u}^{(0)}\to\frac{\mathrm{e}^{i\overline{x}}}{\kappa_y-i|\kappa_z|}\left[\kappa_y\mathrm{e}^{i\kappa_y(2\overline{x})^{1/2}\overline{\eta}-\left(\kappa_z^2+\kappa_y^2\right)\overline{x}}-i|\kappa_z|\mathrm{e}^{-|\kappa_z|(2\overline{x})^{1/2}\overline{\eta}}\right], \tag{15}$$

$$\begin{aligned}\frac{\partial\overline{v}^{(0)}}{\partial\eta}+|\kappa_z|(2\overline{x})^{1/2}\overline{v}^{(0)}\to{}&\frac{i\beta\kappa_z^2\mathrm{e}^{i\overline{x}-|\kappa_z|(2\overline{x})^{1/2}\overline{\eta}}}{(\kappa_y-i|\kappa_z|)\,(2\overline{x})^{1/2}}\\ &+\left[\frac{i\kappa_y\beta\left(\kappa_y^2-\kappa_z^2\right)}{(2\overline{x})^{1/2}\left(\kappa_z^2+\kappa_y^2\right)}-i+\kappa_z^2+\kappa_y^2\right]\mathrm{e}^{i\overline{x}+i\kappa_y(2\overline{x})^{1/2}\overline{\eta}-\left(\kappa_z^2+\kappa_y^2\right)\overline{x}},\end{aligned} \tag{16}$$

$$\frac{\partial\overline{w}^{(0)}}{\partial\eta}+|\kappa_z|(2\overline{x})^{1/2}\overline{w}^{(0)}\to\frac{i\beta|\kappa_z|^3\mathrm{e}^{i\overline{x}-|\kappa_z|(2\overline{x})^{1/2}\overline{\eta}}}{\kappa_y-i|\kappa_z|}-\frac{2\beta\kappa_z^2\kappa_y^2\ \mathrm{e}^{i\overline{x}+i\kappa_y(2\overline{x})^{1/2}\overline{\eta}-\left(\kappa_z^2+\kappa_y^2\right)\overline{x}}}{\kappa_z^2+\kappa_y^2} \tag{17}$$

$$\frac{\partial\overline{p}^{(0)}}{\partial\eta}+|\kappa_z|(2\overline{x})^{1/2}\overline{p}^{(0)}\to-\frac{i\beta|\kappa_z|\mathrm{e}^{i\overline{x}-|\kappa_z|(2\overline{x})^{1/2}\overline{\eta}}}{2\overline{x}\,(\kappa_y-i|\kappa_z|)}+\frac{\beta\kappa_y^2\ \mathrm{e}^{i\overline{x}+i\kappa_y(2\overline{x})^{1/2}\overline{\eta}-\left(\kappa_z^2+\kappa_y^2\right)\overline{x}}}{\overline{x}\left(\kappa_z^2+\kappa_y^2\right)}, \tag{18}$$

and (LWG)

$$\overline{u} = 0, \tag{19}$$

$$\frac{\partial \overline{v}}{\partial \eta} + |\kappa_z|(2\overline{x})^{1/2}\overline{v} \rightarrow -\mathrm{e}^{i\overline{x}+i\kappa_y(2\overline{x})^{1/2}\overline{\eta}-\left(\kappa_z^2+\kappa_y^2\right)\overline{x}}, \tag{20}$$

$$\frac{\partial \overline{w}}{\partial \eta} + |\kappa_z|(2\overline{x})^{1/2}\overline{w} \rightarrow i\kappa_y(2\overline{x})^{1/2}\mathrm{e}^{i\overline{x}+i\kappa_y(2\overline{x})^{1/2}\overline{\eta}-\left(\kappa_z^2+\kappa_y^2\right)\overline{x}}, \tag{21}$$

$$\frac{\partial \overline{p}}{\partial \eta} + |\kappa_z|(2\overline{x})^{1/2}\overline{p} \rightarrow 0, \tag{22}$$

as $\eta \rightarrow \infty$. For a two-dimensional gust, the outer boundary conditions simplify to (2.27)-(2.29) in R09. At the wall, the standard no-slip wall boundary conditions apply to all the velocity components in (10). It has been shown by Gustavsson[28] by use of Darcy's law that such condition is satisfied by the wall-normal velocity component of the disturbance for surfaces with low permeability, a situation often encountered in experiments[17].

For $F_w \gg 1$, asymptotic analysis of the $x-$momentum equation (12) shows that both $\overline{u}^{(0)}$ and $\overline{u}$ satisfy

$$\frac{\partial \overline{u}}{\partial N} + \frac{\partial^2 \overline{u}}{\partial N^2} = 0, \tag{23}$$

where $\epsilon F_w \ll 1$ is assumed to distinguish the mean flow from the disturbance. Note that this condition is reasonable because $\epsilon$, a measure of the turbulence intensity, is about 0.01 or smaller in realistic flow conditions described by linearized equations, and $F_w$ is typically smaller than 10. Furthermore, it is interesting to notice that a large wall suction renders the unsteadiness non influential in the streak dynamics at leading order because of the small size of the viscous region, although the streaks are still modulated in time according to (9). The mechanism is analogous to the quasi-steady dynamics of the streaks when $\overline{x} \ll 1$, where the boundary layer is also very thin.

By applying the no-slip condition and the boundary conditions (15) and (19), the solutions to (23) are[29]

$$\overline{u} = 0, \overline{u}^{(0)} = \frac{\mathrm{e}^{i\overline{x}}\left(1-\mathrm{e}^{-F_w\eta}\right)}{\kappa_y - i|\kappa_z|}\left[\kappa_y \mathrm{e}^{i\kappa_y(2\overline{x})^{1/2}\overline{\eta}-\left(\kappa_z^2+\kappa_y^2\right)\overline{x}} - i|\kappa_z|\mathrm{e}^{-|\kappa_z|(2\overline{x})^{1/2}\overline{\eta}}\right], \tag{24}$$

where the effect of the mean flow in (24) is distilled in $F_w$ and $\beta$, namely the mean flow affects the Klebanoff modes only through its character at the wall (through $F_w$) and in the free-stream (through $\beta$)[30]. Equation (24) shows that a large wall suction can completely suppress the peak of the Klebanoff modes, given by $\overline{u}$. This result will be confirmed by the numerical solution of the LUBR in §III B. The boundary-layer response to a two-dimensional gust is found by setting $\kappa_z = 0$ in (24). We do not carry out asymptotic analysis for massive blowing conditions because for this case a simplified form of the boundary layer equations is found only when an external mean streamwise pressure gradient is present[24].

The LUBR equations (11)-(14) are parabolic in the $\overline{x}$ direction and elliptic in the $z$ direction. They can therefore be solved by marching downstream by applying the initial conditions (B-1)-(B-6) in R09 and (5.25)-(5.27) in LWG, the outer boundary conditions (15)-(22), and the no-slip wall boundary conditions. A second-order, implicit finite-difference scheme is used and the linear system is solved by a standard block-elimination algorithm. A uniform grid with a typical mesh size of $\Delta\eta = 0.03$ is employed and the domain extends to $\eta = 30$. The streamwise step size is $\Delta\overline{x} = 5 \times 10^{-4}$. More details on the computational procedures are found in R09.

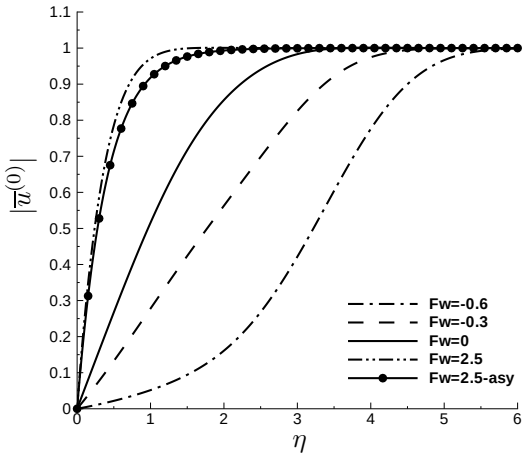


FIG. 3: Profile of $|\overline{u}^{(0)}|$ for $\kappa_z = \kappa_y = 0$ at $\overline{x} = 1$ for different $F_w$. The line with black symbol indicates the analytical solution (24).

## III. RESULTS

### A. Boundary-layer response to a two-dimensional free-stream gust

The effect of wall transpiration on the boundary-layer disturbance induced by a two-dimensional gust is investigated. This form of free-stream disturbance has an infinite spanwise wavelength ($\kappa_z = 0$) and a null spanwise velocity component ($\hat{u}_z^\infty = 0$). Although this type of disturbance may not be of direct interest for practical applications because the free-stream disturbances usually encountered in wind tunnels and in engineering flow systems are inherently three-dimensional, it is undoubtedly important to study them to unravel more fundamental fluid dynamics problems, such as the scattering of TS-waves[31]. Two-dimensional free-stream vortical disturbances have been employed in experimental studies (generated by a vibrating taut platinum ribbon in the free stream, Dietz[32]) and theoretical studies (Choudhari[33], Wu[34]) of receptivity in order to simplify the problem as much as possible, while still preserving the relevant physical features.

We first investigate the case of a gust with a wall-normal wavelength which is large compared with the boundary-layer thickness, i.e. $\kappa_y = 0$. The influence of wall transpiration on the $|\overline{u}^{(0)}|$ profile at $\overline{x} = 1$ is shown in figure 3. The profiles for wall suction and mild wall blowing show similar shapes, with the wall-shear stress increasing with $F_w$. Strong blowing reduces the wall-shear stress significantly and shifts the fluctuations toward the free stream, mainly because the boundary-layer thickens as a result of wall blowing. The effect is analogous to the one on the Blasius mean flow. In support to this observation, we note that, in the limit of large suction, $F_w \gg 1$, the amplitude of the vorticity signature given by the analytical profile (24) for $\kappa_z = \kappa_y = 0$ coincides with $F_{asy}$, the asymptotic solution for the streamwise mean flow given in (7). As depicted in figure 3, the agreement between the analytical solution (24) (black circles) and the numerical solution (dash-dot-dot line) is already good for $F_w = 2.5$, especially near the wall. Wall transpiration has a negligible influence on the wall-normal velocity disturbance profile (not shown), which deviates only slightly from the distribution given by analytical form for locations near the leading edge of the plate ($\overline{x} \ll 1$), i.e. $\overline{v}^{(0)} = (\eta(\eta F')' - F)/(4\overline{x})$ (see equation (4.13) in LWG on page 177).

We now consider free-stream gusts with $\kappa_z = 0$, $\kappa_y = 1$, i.e. with wall-normal wavelength comparable with the boundary-layer thickness, $\lambda_y^* = \mathcal{O}(\delta^*)$ at $\overline{x} = \mathcal{O}(1)$. This represents a more general case compared with the previous one, and it is more involved to investigate experimentally due to the small size of the boundary-layer thickness being comparable with the gust wavelength in common wind-tunnel tests (see R09 for a detailed discussion). One difference from the case with

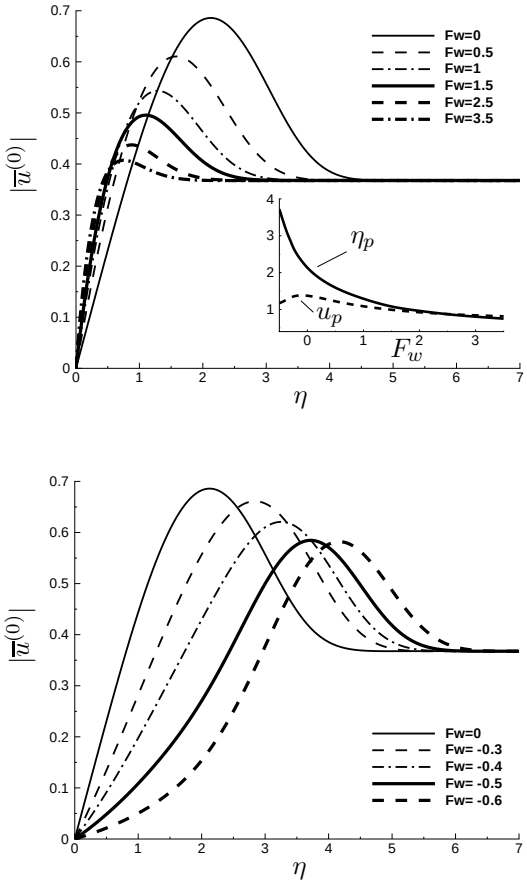


FIG. 4: Profile of $|\overline{u}^{(0)}|$ for $\kappa_z = 0$ and $\kappa_y = 1$ at $\overline{x} = 1$ for wall suction (top) and wall blowing (bottom) for different $F_w$. Inset: amplitude ($\times 2$) ($u_p$ - dashed line) and position ($\eta_p$ - solid line) of $|\overline{u}^{(0)}|$ peak as functions of $F_w$.

$\kappa_z = \kappa_y = 0$ is that the intensity of the free-stream disturbance decays at a fast rate downstream due to viscous effects, while the signature within the boundary layer is amplified relatively to the outer flow because of the stretching imposed by the mean flow. The streamwise velocity profile at $\overline{x} = \mathcal{O}(1)$ therefore presents a peak in the core of the boundary layer. (Note however that there does not yet exist experimental evidence for this two-dimensional case.) Figure 4 shows $|\overline{u}^{(0)}|$ for wall suction (top) and blowing (bottom) at $\overline{x} = 1$. As the suction intensity increases, the fluctuations across the boundary layer are attenuated, and the wall-shear stress of the disturbance increases. Surprisingly, wall blowing also reduces the intensity of the fluctuations for $F_w$ <-0.1. The inset in the bottom graph shows the amplitude $u_p$ and the $\eta_p$ position of the $|\overline{u}^{(0)}|$ peak as functions of $F_w$. The peak moves monotonically toward the wall as $F_w$ increases, and the maximum amplitude is found for very mild blowing, $F_w \approx -0.1$.

Figure 5 presents the comparison between the LUBR suction profiles calculated via the numerical mean flow $F$ (NBR - solid line) and the profiles computed through the asymptotic mean flow solution $F_{asy}$ in (7) (ABR - dashed line). The difference between the NBR and the ABR solutions decreases with increasing $F_w$ as expected, the peaks differing by only 1% for $F_w = 3.5$. The lines with symbols in figure 5 indicate the numerical calculations with $F_{asy}$ (black circles) and the full asymptotic solution (24) (white circle) for $F_w = 10$. This shows that an intense wall suction is required to suppress the peak in the core of the boundary layer at $\overline{x} = 1$, as predicted by the asymptotic theory.

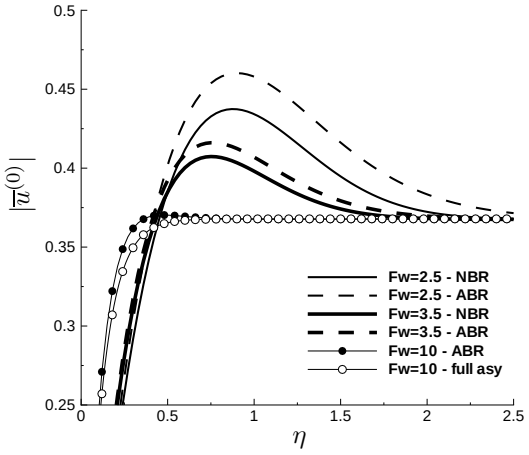


FIG. 5: Profile of $|\overline{u}^{(0)}|$ for $\kappa_z = 0$ and $\kappa_y = 1$ at $\overline{x} = 1$ for different $F_w$. NBR indicates the full numerical LUBR solution, and ABR denotes the numerical solution computed with $F_{asy}$.

Figures 6, 7 and 8 show the $|\overline{u}^{(0)}|$ and $|\overline{v}^{(0)}|$ velocity profiles at different $\overline{x}$ for $F_w = -0.25, 0, 1.5$, respectively. Suction attenuates the intensity of the streamwise velocity fluctuations (shown on the top graphs), while the effect of blowing is very mild on the energy of this velocity component for a blowing intensity $F_w = -0.25$. As $\overline{x}$ increases, the peak of the $|\overline{u}^{(0)}|$ profiles moves upward for blowing ($\eta \approx 3$ at $\overline{x} = 2.5$). Blowing amplifies the amplitude of the $\overline{v}^{(0)}$ fluctuations (shown on the bottom graphs) at small $\overline{x}$ and has little effect at larger $\overline{x}$. Suction intensifies $|\overline{v}^{(0)}|$ near the leading edge and damps it further downstream. Note however that near the leading edge $|\overline{v}^{(0)}|$ decreases with respect to the local mean $V$, which is large there because of the similarity form given in (6).

### B. Boundary-layer response to three-dimensional free-stream gusts: the Klebanoff modes

The influence of wall suction and blowing on the Klebanoff modes, namely disturbances induced by three-dimensional gusts, is studied. This case represents the one that is most relevant to practical applications because free-stream turbulence with small intensity level (typically with root mean square (rms) smaller than 1% of the free-stream velocity) can be viewed mathematically as a composite spectrum of unsteady, three-dimensional vortical fluctuations of the gust type. In experimental studies, full-spectrum free-stream turbulence is the most commonly employed generator of three-dimensional unsteady Klebanoff modes to date, while experimental studies on *single* Klebanoff modes (for example three-dimensional versions of Dietz's analysis) are still lacking.

As the flow is now three-dimensional, we consider the full disturbance solution $\{\overline{u}_0, \overline{v}_0, \overline{w}_0, \overline{p}_0\}$, given in (10). For the first cases, the flow parameters are $\kappa_z = \kappa_y = 1$ ($\lambda_y^* = \lambda_z^* = \mathcal{O}(\delta^*)$ at $\overline{x} = \mathcal{O}(1)$), and $k_x = 0.1$ and $\hat{u}_z^\infty = -0.2$. From (1) and (2), it follows that $k_y = 2\pi$, $\hat{u}_x^\infty \approx 0.96$, $\hat{u}_y^\infty \approx 0.18$, and $R_\lambda \approx 394.8$. This flow setting matches a possible, realistic wind-tunnel situation because it has been amply documented that, when the downstream distance is sufficiently large, the Klebanoff modes typically present spanwise length scales comparable with the local boundary-layer thickness[6]. In R09, the same flow conditions were studied, for which $\overline{u}$ dominates in the core of the boundary layer (as first shown by LWG), while $\overline{u}^{(0)}$ is relevant near the free stream and matches the streamwise free-stream velocity (as first shown by Choudhari[33]).

Figure 9 shows $|\overline{u}_0|$ (top) and $|\overline{v}_0|$ (bottom) for wall suction and blowing conditions at $\overline{x} = 1$. The intensity of the streamwise velocity fluctuations is significantly reduced by wall suction and intensified by wall blowing. The effect is more intense than on two-dimensional disturbances: the peak in the middle of the boundary layer disappears for $F_w > 2$, i.e. for lower values of $F_w$ than

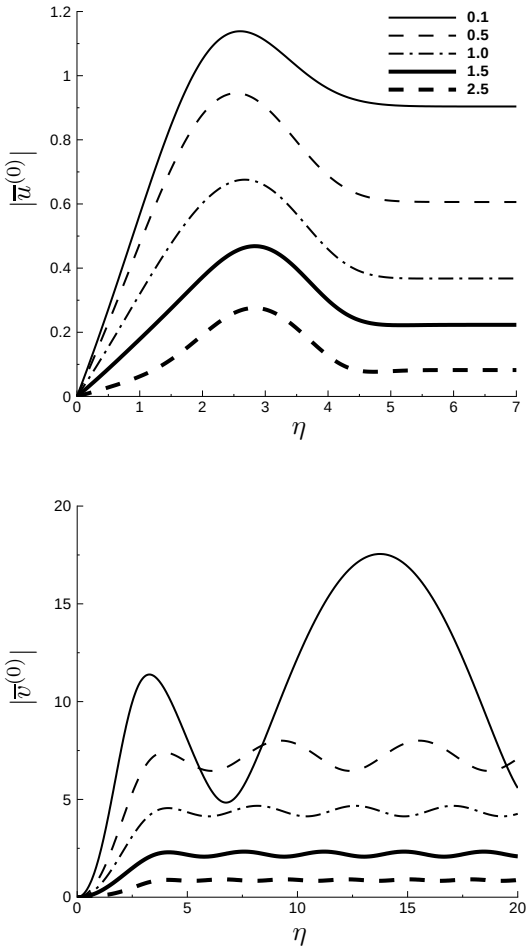


FIG. 6: Profiles of $|\overline{u}^{(0)}|$ (top) and $|\overline{v}^{(0)}|$ (bottom) at $F_w = -0.25$ for $\kappa_z = 0$, $\kappa_y = 1$ at different $\overline{x}$.

in the two-dimensional case. The location of the $|\overline{u}_0|$ maximum moves closer to the wall as $F_w$ increases. The $\overline{v}_0$ fluctuations behave similarly to $\overline{u}_0$, if exception is made for $F_w > 0.5$, for which $|\overline{v}_0|$ is slightly intensified in the middle of the viscous region. The spanwise velocity fluctuations, shown in figure 10 (top), are brought closer to the wall by wall suction (and slightly intensified). The two maxima in the $|\overline{w}_0|$ profile are both shifted upward ($\eta \approx 2.5$ and $\eta \approx 5.5$). Figure 10 (bottom) shows that wall suction intensifies the pressure disturbance $\overline{p}_0$ at and near the wall, and attenuates them in the outer part, while blowing has the opposite effect. The pressure peak in the core of the boundary layer appears for $F_w \leq 0$ (and for mild suction), and it is located at the same wall-normal location of the $|\overline{u}_0|$ peak.

The effect of the disturbance frequency $k_x^* U_\infty$ is studied. We compare the results with a reference case, i.e. $\kappa_{z,ref} = \kappa_{y,ref} = \overline{x} = 1$ and $k_{x,ref} = 0.1$, and compute the flow conditions by $\kappa_{z,new} = \kappa_{y,new} = \kappa_{z,ref}(k_{x,ref}/k_{x,new})^{1/2}$. (Given that $\overline{x} = k_x x$, we also modify $\overline{x}$ to ensure that we study the disturbances at the same location downstream.) Figures 11 and 12 show the influence of $F_w$ on $|\overline{u}_0|$ and $|\overline{w}_0|$ for $k_x = 0.2$ (top graphs) and $k_x = 0.8$ (bottom graphs). Wall suction has an intense attenuating effect on low-frequency $|\overline{u}_0|$ disturbances. High-frequency fluctuations are instead not greatly modified in magnitude as they are confined in the outer part of the boundary layer and therefore far from the suction wall. They are however more significantly shifted vertically than the low-frequency ones. The spanwise velocity component in figure 12 is much less affected, and so is

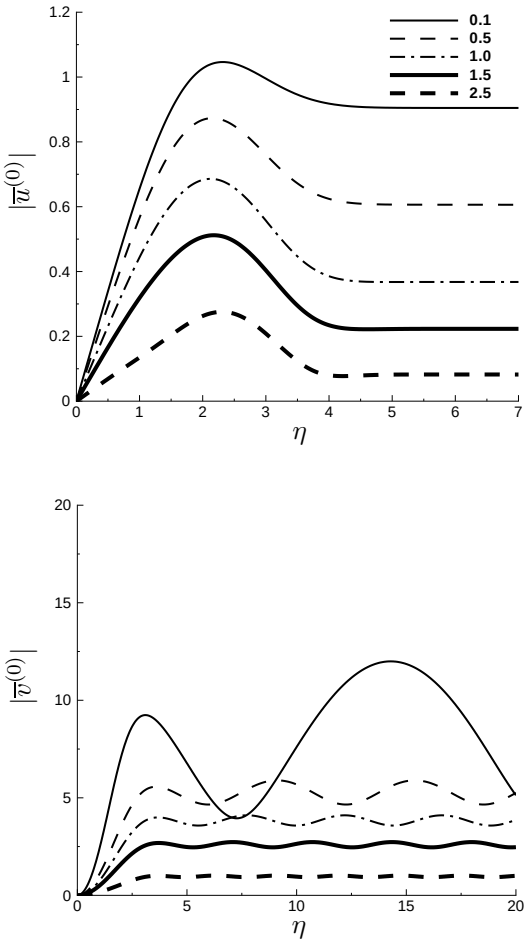


FIG. 7: Profiles of $|\overline{u}^{(0)}|$ (top) and $|\overline{v}^{(0)}|$ (bottom) at $F_w = 0$ for $\kappa_z = 0$, $\kappa_y = 1$ at different $\overline{x}$.

the wall-normal one (not shown). Figure 13 (top) shows that the full numerical solution and the numerical solution obtained with the asymptotic mean-flow solution (7) agree satisfactorily already for $F_w = 2.5$. Figure 13 (bottom) indicates that a good comparison with the full asymptotic solution (24) is achieved only for higher suction intensity, $F_w = 10$.

We now proceed to study the downstream evolution of the maximum of the rms of the streamwise velocity fluctuations. The following mathematical framework has been developed by LWG and used further by Ricco & Wu[13]. The free-stream turbulence can be represented by a continuous band of Fourier components. Because of linearity, the boundary-layer fluctuations are computed by adding the contribution of each Fourier component to obtain the rms of the streamwise velocity component. The mean-square streamwise velocity fluctuation produced by a broadband free-stream turbulence is given by

$$< u'^2 > (R_\lambda, \eta, \delta) = \frac{R_\lambda}{\delta^2} \int_0^\infty \Phi_t(k_x = 0, \xi/\delta) K_\infty(\xi, \eta) \xi \mathrm{d}\xi, \tag{25}$$

where $\epsilon u' \equiv u - F'$, $<>$ indicates the mean value, $\delta = \delta^*/\lambda_z^*$, and

$$K_\infty(\xi, \eta) = 2 \int_0^\infty \int_0^{2\pi} \frac{\sin^2\theta}{s^2} |\overline{u}(\overline{x}, \eta, \theta, s)|^2 \, \mathrm{d}\theta \, \mathrm{d}s. \tag{26}$$

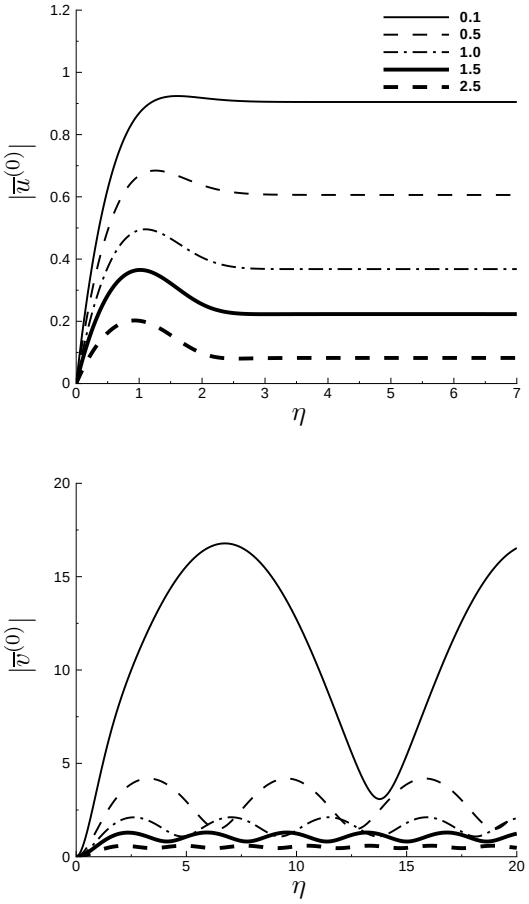


FIG. 8: Profiles of $|\overline{u}^{(0)}|$ (top) and $|\overline{v}^{(0)}|$ (bottom) at $F_w = 1.5$ for $\kappa_z = 0$, $\kappa_y = 1$ at different $\overline{x}$.

Only $\overline{u}$ is retained for the streamwise velocity component because we are interested in the Klebanoff mode signature in the core of the boundary layer, where $\overline{u}$ is of leading order. The quantities $\xi$, $\theta$ and $s$ are related to $k_y$, $k_z$ and $\overline{x}$ via the relations: $\{k_y, k_z\} = \xi\{\cos\theta, \sin\theta\}/\delta$, $\overline{x} = \xi^2 s/2$, $\delta = \sqrt{2x/R_\lambda}$, from which it follows $\xi = \delta\Gamma$, $\{\kappa_z, \kappa_y\} = \{\sin\theta, \cos\theta\}/\sqrt{s}$, $s = k_x R_\lambda \delta^2/\xi^2$. In (25), $\Phi_t(\xi/\delta)$ is the spectrum of the free-stream turbulence. We employ the following form of $\Phi_t$:

$$\Phi_t(\xi/\delta) = \frac{D < u_\infty^2 >}{\pi^2 \delta^2} \xi^2 \mathrm{e}^{-(\xi/\delta - \overline{k}_I)^2/\Delta},$$

where $\Delta = 4.0$, $\overline{k}_I = -7.0$, and $D$ is a constant. This function has been used by LWG to study the experimental data by Kendall, unpublished before then (see page 192 in their paper). In order to compute the rms in a frequency band $\{k_{1L}, k_{1H}\}$, the function (26) is modified as follows:

$$K_{<>}(\xi, \eta; \delta, R_\lambda, k_{1L}, k_{1H}) = 2 \int_{s_L}^{s_H} \int_0^{2\pi} \frac{\sin^2\theta}{s^2} |\overline{u}(\overline{x}, \eta, \theta, s)|^2 \, \mathrm{d}\theta \, \mathrm{d}s,$$

where $\{s_L, s_H\} = \{k_{1L}, k_{1H}\} R_\lambda \delta^2/\xi^2$.

The above theoretical framework is used to study the effect of suction on the rms of the streamwise velocity fluctuations in Kendall's experiment. The flow conditions are $U_\infty = 11.6$ m/s, a spanwise integral length scale $\Lambda_z^* = 0.009$ m and a free-stream turbulence level of about $Tu = 0.26\%$

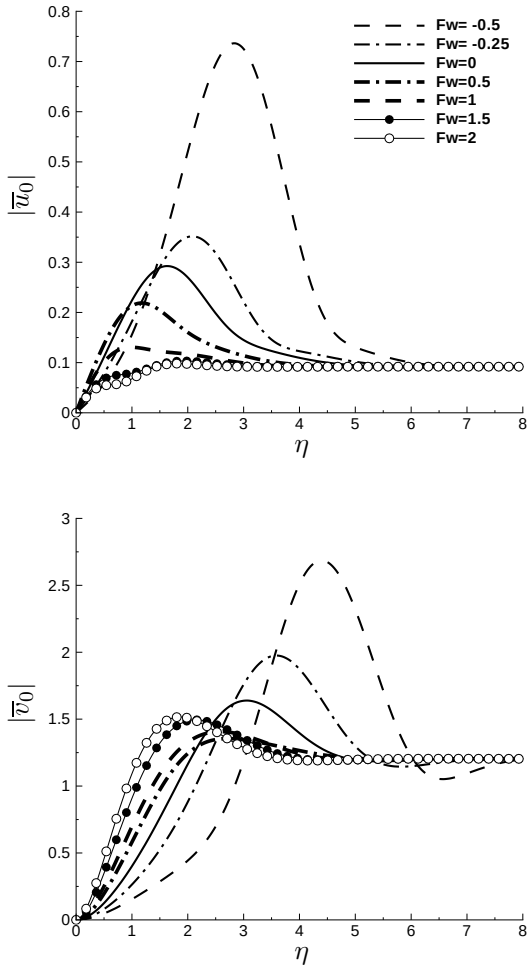


FIG. 9: Profiles of $|\overline{u}_0|$ (top) and $|\overline{v}_0|$ (bottom) for $\kappa_z = \kappa_y = 1$, $k_x = 0.1$, $\hat{u}_z^\infty = -0.2$ and $\overline{x} = 1$ for different $F_w$. The legend also applies to figures 10 through 12.

($\epsilon R_\lambda = 17.4$, where henceforth $R_\lambda = U_\infty \Lambda_z^*/\nu$). Figure 14 shows the rms of the streamwise velocity fluctuation at $\eta = 1.64$ (which roughly corresponds to the wall-normal peak) as a function of $x$ for different frequency bands and for $F_w = 0, 1, 2$. Wall suction significantly attenuates the full-spectrum rms, and the effect is comparable for the three frequency bands up to $x \approx 50$. Further downstream, low-frequency disturbances are suppressed, but the rms at higher frequencies are intensified. By observing figure 11, it is clear that high-frequency fluctuations are enhanced in the core of the boundary layer because the profile is brought closer to the wall.

The above results compare qualitatively with the experimental data of the $x$-dependence of the $u_{rms}$ maximum presented by Yoshioka, Fransson & Alfredsson[18] (YFA) in figure 9 at page 3535 of their paper. No detailed quantitative comparison of the streak streamwise evolution is possible because no precise information on the free-stream spectrum is provided for the experimental tests. The wall velocity distribution is different in the two settings, i.e. ASBL in their case and similarity solution in ours. However, the spanwise integral length scales $\Lambda^*$ are similar, 7.5 mm for YFA and 9 mm for our calculations, and the measurement locations are comparable, about 2 m of streamwise distance from the leading edge. The intensities of wall transpiration are also similar. In the range where the streaks are fully developed, i.e. where $\delta^*$ is comparable with $\Lambda_z^*$, i.e. for 100< $x$ <300 in

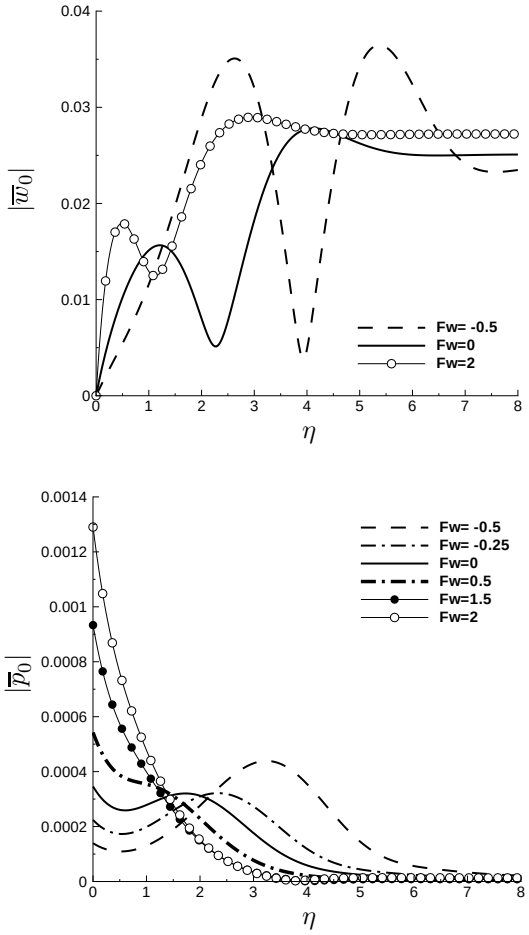


FIG. 10: Profiles of $|\overline{w}_0|$ (top) and $|\overline{p}_0|$ (bottom) for $\kappa_z = \kappa_y = 1$, $k_x = 0.1$, $\hat{u}_z^\infty = -0.2$ and $\overline{x} = 1$ for different $F_w$.

figure 14, the amplitude of wall transpiration for $F_w = 2$ varies between 0.17% and 0.11% of $U_\infty$, which would correspond to an intermediate case in YFA's experiments comprised between their data indicated by an inverted triangle and a square in their figure 9 at page 3535. Along this streamwise extent, which roughly corresponds to 0.7 m$< x^* <$2.0 m in YFA's experiment, the trends are similar in shape, but YFA show a 50% rms reduction, while our calculations indicate a 75% attenuation. This discrepancy may be due to two factors. Nonlinear effects, neglected in our calculations, are likely to be relevant in YFA's tests because of their higher free-stream turbulence level, $Tu = 1.5-2\%$ ($\epsilon R_\lambda = 36.1$), than in our calculations, $Tu = 0.26\%$. Secondly, the similarity form of wall velocity distribution is likely to induce higher reductions because, although the intensity of the transpiration along the measurement location is similar to the experimental case, in the latter the leading edge region is without transpiration.

Figure 15 shows the effect of wall suction on the rms profile of the Klebanoff modes measured by Westin *et al.*[6] (WEA). The wall-normal direction is $\overline{Y} = y^*/\delta_1^*$, where $\delta_1^*$ is the displacement thickness in each case. The procedure to calculate the rms is described in R09 at pages 22-25 and it involves the summation of wall-normal distributions at different frequencies. The only computational difference is that the mean flow is modified to account for the suction. The attenuation is less intense than on the rms of Kendall. We can use these results for comparison with the ASBL rms data measured by Fransson & Alfredsson[17] (FA). Indeed, these tests were conducted in the same

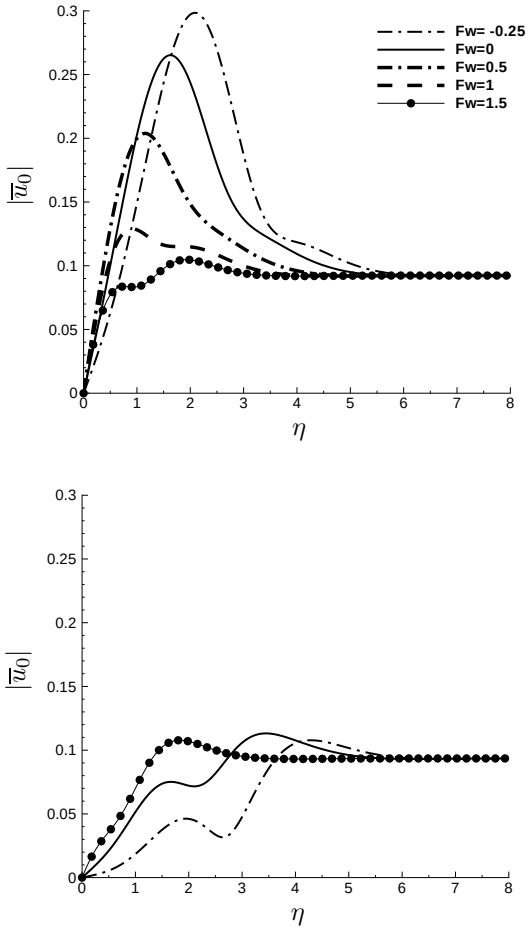


FIG. 11: Profiles of $|\overline{u}_0|$ for $k_x = 0.2$ at $\overline{x} = 2$ (top) and $k_x = 0.8$ at $\overline{x} = 8$ (bottom) for different $F_w$.

wind-tunnel facility and most of the flow conditions are very similar. The free-stream turbulence level was about 1% for both, and the spanwise length scales were of comparable magnitude, about 7 mm for WEA and about 9 mm for FA ($\epsilon R_\lambda = 35.9$ and 28.9, respectively). The free-stream velocity was $U_\infty = 8$ m/s for WEA and $U_\infty = 5$ m/s for FA, so that it is best to consider the FA's data at $x^* = 800$ mm for comparison with WEA's data at $x^* = 500$ mm in order to have the same streamwise Reynolds number, $Re_x = x^* U_\infty/\nu$ =255100. This also allows us to compute $F_w \approx 2$ to have the same suction velocity at the measurement location. Despite the fact that FA considered ASBL condition, while we study the similarity form of wall suction, the comparison between our numerical calculations and FA's experimental data is good. The peak of the rms decreases by about 45% in our calculations and by about 31% in FA's case, and the maximum location changes from $\overline{Y}$=1.5 to 1.2 in our calculations, and from $\overline{Y}$=1.3 to 1.1 in FA's experiment (compare data in figures 31 and 32 in their paper). Similarly to the analysis of Kendall's data, the percent attenuation is predicted to be larger than in the experimental studies, which is likely to be primarily due to the wall distribution of suction rather than on nonlinear effects, because the $Tu$ level was medium and comparable ($\sim$1%) in the two cases.

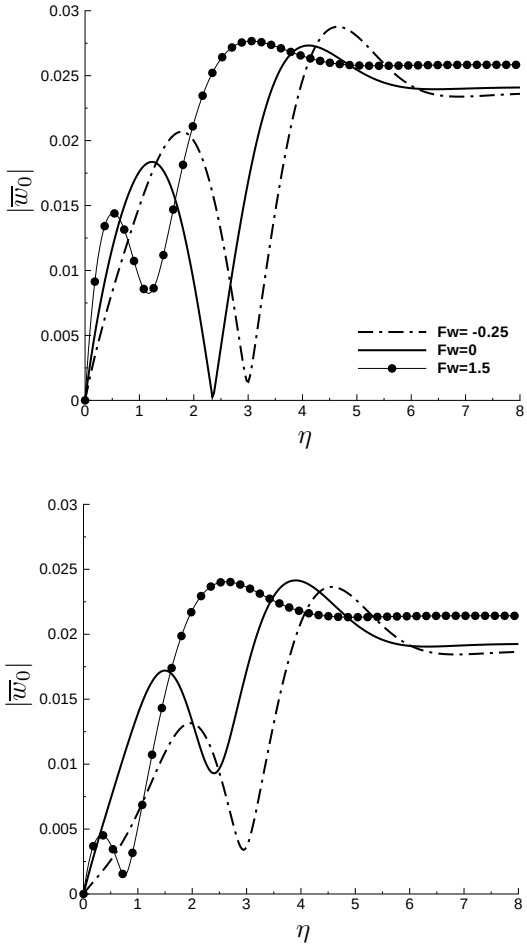


FIG. 12: Profiles of $|\overline{w}_0|$ for $k_x = 0.2$ at $\overline{x} = 2$ (top) and $k_x = 0.8$ at $\overline{x} = 8$ (bottom) for different $F_w$.

## IV. SUMMARY AND OUTLOOK

The effect of mean-flow wall transpiration on the laminar streaks, namely unsteady vorticity disturbances engendered in the incompressible Blasius boundary layer by free-stream vortical fluctuations, has been investigated numerically. An asymptotic solution for the streak profile for large suction intensity has been compared successfully with the numerical solution. This analysis has revealed that in this limit the unsteadiness is non influential in the streak dynamics and that the free-stream streamwise velocity of the disturbance decreases exponentially to zero as the wall is approached, with the rate of decay proportional to the mean-flow suction intensity. The peak in the core of the boundary layer, i.e. the distinguished feature of the Klebanoff mode profile[7], may be completely suppressed by large suction.

Wall suction attenuates both two- and three-dimensional fluctuations and shifts the profiles closer to the wall. Blowing moves the disturbances toward the free stream and enhances three-dimensional fluctuations. Unexpectedly, it can damp two-dimensional disturbances if sufficiently intense. Low-frequency Klebanoff modes are much more modified by wall transpiration than high-frequency ones, which are not affected in amplitude, but are simply shifted wallward by suction and upward by blowing. Pressure disturbances are found to be intensified near the wall by suction. The analysis has highlighted the importance of the precise specification of the free-stream disturbances when

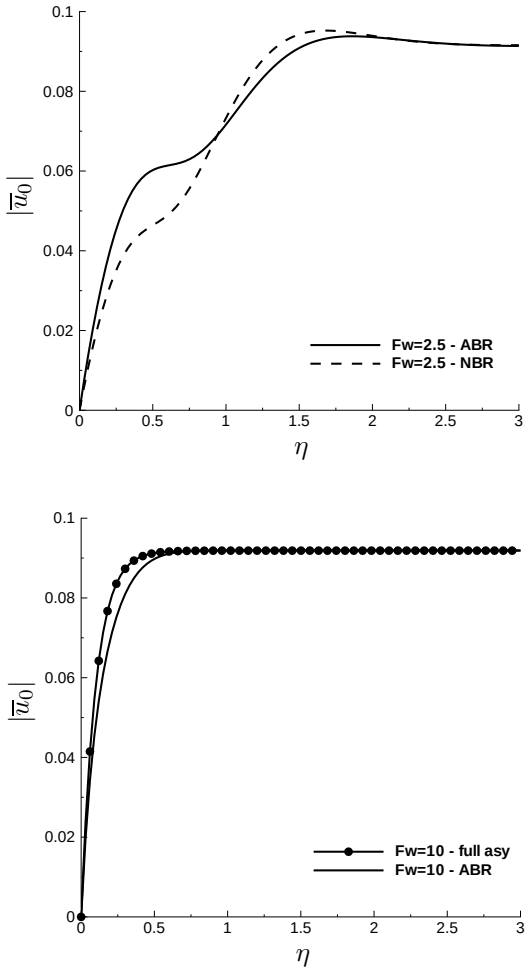


FIG. 13: Comparison of streamwise $|\overline{u}_0|$ velocity flucuations profiles at $\overline{x} = 1$ for $F_w = 2.5$ (top) using numerical (NBR) and asymptotic mean-flow (ABR) solutions, and for $F_w = 10$ using asymptotic mean-flow (ABR) solution and full asymptotic solution (24).

studying the laminar streaks.

We have furthermore carried out numerical thought experiments on the influence of wall suction on the wind-tunnel data by Kendall (published in LWG and Ricco & Wu[13]) and by Westin *et al.*[6], conducted in no-transpiration conditions, thereby showing the attenuation of the rms of the full-spectrum laminar streaks. This analysis has also proved useful for comparison with experimental data with suction by Yoshioka, Fransson & Alfredsson[18] and by Fransson & Alfredsson[17]. The quantitative discrepancies have been attributed to nonlinear effects, likely to play a decisive role because of the free-stream turbulence level, and to the wall velocity distribution, ASBL in the experiments and self-similarity in our case.

We conclude this paper by outlining some possible ideas for future research work. Experimental tests should probably focus more on the detailed description of the free-stream oncoming turbulence, such as spectrum and scales, in order to validate and improve the theoretical approach and allow for further quantitative comparisons. The boundary-layer response to free-stream disturbances with more controllable characteristics, for example with a very narrow frequency band, would also be of interest. The recent papers by Pan *et al.*[35] and Wang, Pan & Zhang[36], where laminar streaks

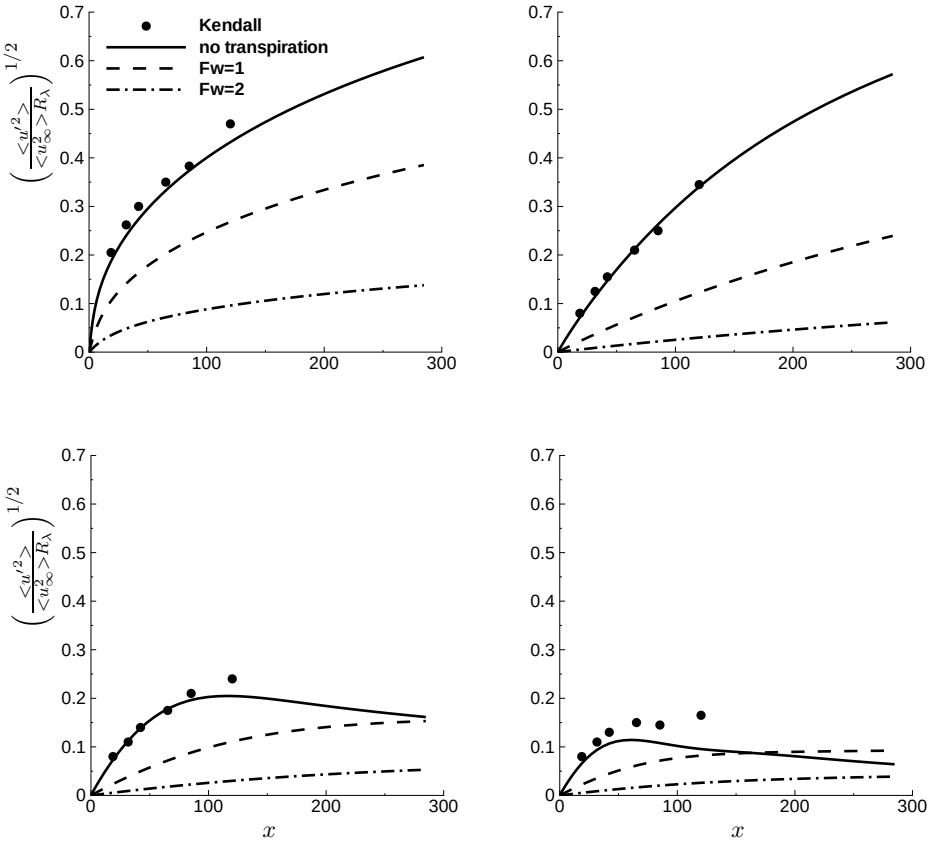


FIG. 14: Experimental data by Kendall with no wall suction and numerical results at $\eta = 1.64$ with no transpiration and with $F_w = 1, 2$. From left to right and from top to bottom: broadband rms; rms for $f^* = \{0, 4\}$ Hz; rms for $f^* = \{4, 8\}$ Hz and rms for $f^* = \{8, 12\}$ Hz.

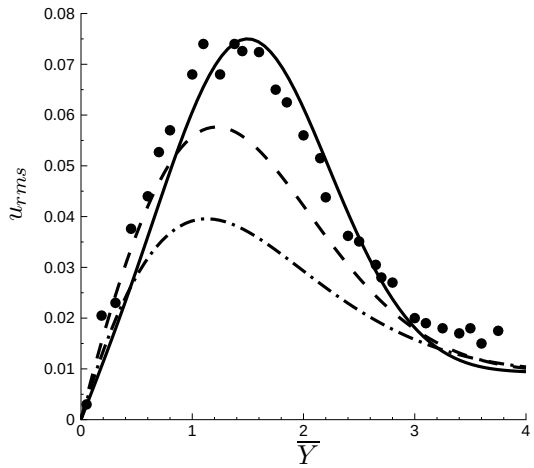


FIG. 15: Rms profile of streamwise velocity fluctuation for Westin *et al.*[6] (black circles), and present numerical calculations: $F_w = 0$ (solid line), $F_w = 1$ (dashed line), $F_w = 2$ (dot-dashed line).

generated by wakes shed from vertically positioned cylinders have been studied, are first steps toward this direction. It would also be interesting to verify experimentally the asymptotic result that the peak of the Klebanoff modes can be suppressed completely for sufficiently intense wall suction, to modify the present mathematical framework to investigate the ASBL case, and to extend it to account for nonlinear effects to achieve a better agreement with experimental data.

**Acknowledgements**

We would like to thank Dr G. Papadakis for reading a preliminary version of the paper and for his useful comments.

**References**

[1] M. E. Goldstein and L. S. Hultgren. Boundary layer receptivity to long-wave free-stream disturbances. *Ann. Rev. Fluid Mech.*, 21:137–166, 1989.
[2] R. D. Joslin. Aircraft laminar flow control. *Ann. Rev. Fluid Mech.*, 30:1–29, 1998.
[3] P. S. Klebanoff. Effect of free-stream turbulence on a laminar boundary layer. *Bull. Am. Phys. Soc.*, 16:1323, 1971.
[4] H. L. Dryden. Air flow in the boundary layer near a plate. *NACA Rep.*, 562, 1936.
[5] G. I. Taylor. Some recent developments in the study of turbulence. *Fifth Intl. Congr. for Appl. Mech., ed. J.P. Den Hartog & Peters, Wiley/Chapman and Hall, New York-London*, pages 294–310, 1939.
[6] K. J. A. Westin, A. V. Boiko, B. G. B. Klingmann, V. V. Kozlov, and P. H. Alfredsson. Experiments in a boundary layer subjected to free stream turbulence. Part 1. Boundary layer structure and receptivity. *J. Fluid Mech.*, 281:193–218, 1994.
[7] M. Matsubara and P. H. Alfredsson. Disturbance growth in boundary layers subjected to free-stream turbulence. *J. Fluid Mech.*, 430:149–168, 2001.
[8] R. G. Jacobs and P. A. Durbin. Simulation of bypass transition *J. Fluid Mech.*, 428:185–212, 2001.
[9] V. Ovchinnikov, M. M.Choudhari, and U. Piomelli. Numerical simulations of boundary-layer bypass transition due to high-amplitude free-stream turbulence *J. Fluid Mech.*, 613:135–169, 2008.
[10] S. J. Leib, D. W. Wundrow, and M. E. Goldstein. Effect of free-stream turbulence and other vortical disturbances on a laminar boundary layer. *J. Fluid Mech.*, 380:169–203, 1999.
[11] D. W. Wundrow and M. E. Goldstein. Effect on a laminar boundary layer of small-amplitude streamwise vorticity in the upstream flow. *J. Fluid Mech.*, 426:229–262, 2001.
[12] X. Wu and M. Choudhari. Linear and non-linear instabilities of a Blasius boundary layer perturbed by streamwise vortices. Part 2. Intermittent instability induced by long-wavelength Klebanoff modes. *J. Fluid Mech.*, 483:249–286, 2003.
[13] P. Ricco and X. Wu. Response of a compressible laminar boundary layer to free-stream vortical disturbances. *J. Fluid Mech.*, 587:97–138, 2007.
[14] P. Ricco, D.-L. Tran, and G Ye. Wall heat transfer effects on Klebanoff modes and Tollmien-Schlichting waves in a compressible boundary layer. *Phys. Fluids*, 21:024106, 2009.
[15] P. Ricco. The pre-transitional Klebanoff modes and other boundary-layer disturbances induced by small-wavelength free-stream vorticity. *J. Fluid Mech.*, 638:267–303, 2009.
[16] P. Ricco. Asymptotic theory of the pre-transitional laminar streaks and comparison with experiments. *Proc. of $7^{th}$ IUTAM Symposium on Laminar-Turbulent Transition, Stockholm, Sweden, 2009, Ed. P. Schlatter & D. Henningson, Springer.*
[17] J. H. M. Fransson and P. H. Alfredsson. On the disturbance growth in an asymptotic suction boundary layer *J. Fluid Mech.*, 482:51–90, 2003.
[18] S. Yoshioka, J. H. M. Fransson, and P. Alfredsson. Free stream turbulence induced disturbances in boundary layers with wall suction. *Phys. Fluids*, 16,10:3530–3539, 2004.

[19] O. Levin, E. N. Davidsson, and D. Henningson. Transition thresholds in the asymptotic suction boundary layer. *Phys. Fluids*, 17:114104, 2005.
[20] E. N. Davidsson and Gustavsson, L. H. Elementary solutions for streaky structures in boundary layers with and without suction. *Fluid Dyn. Res.*, 40,3:212-231, 2008.
[21] J. H. M. Fransson and P. Corbett. Optimal linear growth in the asymptotic suction boundary layer. *Eur. J. Mech. B/Fluids*, 22:259–270, 2003.
[22] S. Zuccher, P. Luchini, and A. Bottaro Algebraic growth in a Blasius boundary layer: optimal and robust control by mean suction in the nonlinear regime. *J. Fluid Mech.*, 513:135-160, 2004.
[23] M. Bystrom, O. Levin, and D. Henningson. Optimal disturbances in suction boundary layers. *Eur. J. Mech. B/Fluids*, 26,3:330–343, 2006.
[24] H. Schlichting and K. Gersten. *Boundary-Layer Theory.* Springer-Verlag Berlin Heidelberg, 2000.
[25] D. R. Kassoy. On laminar boundary layer separation due to mass injection. *SIAM Appl. Mech.*, 18:29–40, 1970.
[26] A. N. Gulyaev, V. E. Kozlov, V. R. Kuzenetsov, B. I. Mineev, and A. N. Sekundov. Interaction of a laminar boundary layer with external turbulence. *Izv, Akad. Navk. SSSR Mekh. Zhid. Gaza 6*, pages 700–710, 1989.
[27] N. Kemp. The laminar three-dimensional boundary layer and a study of the flow past a side edge. *MAcs Thesis, Cornell University*, 1951.
[28] C. Gustavsson. Development of three-dimensional disturbances in boundary layers with suction. *Master Thesis, Lulea University of Technology, Lulea, Sweden*, 017, 2000.
[29] The second solution in (24) satisfies (23) by neglecting terms $\mathcal{O}(F_w^{-1})$.
[30] Note however that $F_w$ and $\beta$ coincide in absolute value as $F_w \to \infty$ because $V = V_w$ across the boundary layer (see (7)).
[31] X. Wu. Receptivity of boundary layers with distributed roughness to vortical and acoustic disturbances: A second-order asymptotic theory and comparison with experiments *J. Fluid Mech.*, 431,91–133, 2001.
[32] A. J. Dietz. Local boundary-layer receptivity to a convected free-stream disturbance. *J. Fluid Mech.*, 378,291-317, 1999.
[33] M. Choudhari. Boundary layer receptivity to three-dimensional unsteady vortical disturbances in the free stream. *AIAA Paper*, 96-0181, 1996.
[34] X. Wu. On local boundary-layer receptivity to vortical disturbances in the free-stream *J. Fluid Mech.*, 449,373-393, 2001.
[35] C. Pan, J. J. Wang, P. F. Zhang, and L. H. Feng. Coherent structures in bypass transition induced by a cylinder wake. *J. Fluid Mech.*, 603: 367-389, 2008.
[36] J. J. Wang, C. Pan, and P. F. Zhang. On the instability and reproduction mechanism of a laminar streak. *J. Turbul.*, 10,26: 1-27, 2009.